HOT SURFACE IGNITION OF HYDROGEN-AIR MIXTURES

Melguizo-Gavilanes, J., Mével, R., and Shepherd, J.E.

Explosion Dynamics Laboratory
Graduate Aerospace Laboratories of the California Institute of Technology (GALCIT)
Pasadena, CA, USA, josuemg@caltech.edu

ABSTRACT

Hot surface ignition is relevant in the context of industrial safety. In the present work, two-dimensional simulations with detailed chemistry, and study of the reaction pathways of the buoyancy-driven flow and ignition of a stoichiometric hydrogen-air mixture by a rapidly heated surface (glowplug) are reported. Experimentally, in hydrocarbon-air, ignition is observed to occur regularly at the top of the glowplug; numerical results for hydrogen-air reproduce this trend, and shed light on this behavior. Flow separation plays a crucial role in creating zones where convective losses are minimized and heat diffusion is maximized, resulting in the critical conditions for ignition to take place.

1. INTRODUCTION

Ignition of combustible atmospheres by hot surfaces is a common issue in industrial safety. Determining critical conditions for ignition in terms of surface size and temperature are essential in order to evaluate the potential of an ignition hazard. Classical experimental work on hot surface ignition includes that of Coward and Guest [1], and Kutcha [2]. The former investigated the effect of material (e.g catalytic and non-catalytic surfaces) on ignition thresholds, whereas the latter extended this work to study the effect of variations in size and geometry. The impact of their results was hindered by their inability to measure flow velocity and composition during the ignition event. An extensive review of more recent studies is given by Brabauskas [3]. Experimental work done by Boettcher [4] using a glow plug found the ignition temperature for n-Hexane to be essentially insensitive to composition away from flammability limits. Analytical studies have been performed by Gray [5] who investigated the effect of surface to volume ratio, and more recently Laurendeau [6] in which a simple model is proposed to estimate the minimum ignition temperature. Some numerical efforts in this area are due to Kumar [7] who developed a one-dimensional model to study hydrogen ignition, and the two-dimensional steady simulations of Adler [8] in which the problem of a circular hot spot in contact with reactive mixture was analyzed. Boettcher [4] carried out simulations to examine predicting lower flammability limits with tabulated chemistry as well as studying the effect of hot surface area on ignition temperature using one-step and detailed chemical reactive models [9].

None of the previous work has been concerned with analyzing in detail the flow field in the vicinity of the hot surface. For an accurate numerical prediction of this flow, it is necessary to solve the conservation equations together with transport of chemical species on a mesh small enough to capture the thermal and hydrodynamic boundary layer surrounding the hot surface. The wide range of temporal and spatial scales involved, as well as the size of detailed chemical kinetic mechanisms pose significant computational

challenges. Hydrogen is one of the fuels for which the chemistry is better known, the detailed kinetic mechanism is of a reasonable size to simulate realistic geometries, and constitutes a good model fuel for understanding the kinetics of complex hydrocarbons. A two-dimensional numerical simulation of the transient viscous flow and ignition of combustible atmospheres using a detailed hydrogen oxidation mechanism is presented. Special attention is given to the near-wall buoyancy flow induced, and flow separation to gain insight on the dynamics, time and location of the ignition event.

2. PHYSICAL MODEL, NUMERICAL APPROACH AND SIMULATION PARAMETERS

The heat transfer and ignition process in the gas is modeled by the variable-density reactive Navier-Stokes equations with temperature dependent transport properties.

$$\frac{\partial \rho}{\partial t} + \nabla \cdot (\rho \mathbf{u}) = 0 \tag{1}$$

$$\frac{\partial (\rho \mathbf{u})}{\partial t} + \nabla \cdot (\rho \mathbf{u}\mathbf{u}) = -\nabla p + \nabla \cdot \tau + \rho \mathbf{g} \tag{2}$$

$$\frac{\partial (\rho h)}{\partial t} + \nabla \cdot (\rho \mathbf{u} h) = \nabla \cdot (\kappa / c_p \nabla h) + q_{chem} + \frac{Dp}{Dt} \tag{3}$$

$$\frac{\partial (\rho Y_i)}{\partial t} + \nabla \cdot (\rho \mathbf{u} Y_i) = \nabla \cdot (\rho D_i \nabla Y_i) + \Omega_i \tag{4}$$

$$\text{with } \; p = \rho \bar{R} T, \;\; \tau = (p + \frac{2}{3}\mu \nabla \cdot \mathbf{u})\mathbf{I} + \mu[\nabla \mathbf{u} + (\nabla \mathbf{u})^T] \tag{5}$$

The Sutherland Law, the Eucken Relation and the JANAF polynomials are used to account for the functional temperature dependence of mixture viscosity (μ), thermal conductivity (κ) and specific heat (c_p) respectively. The chemistry is modeled using Mevel's detailed mechanism for hydrogen oxidation which includes 9 species and 21 reactions [10, 11] . In equations (1)-(5), ρ is density, $\mathbf{u}$ is the velocity vector, p is pressure, T is the gas temperature, h is the mixture enthalpy, g is the gravitational acceleration, $q_{chem} = \sum h_i \Omega_i$ is the chemical energy conversion rate, Y_i is the mass fraction of species, $\Omega_i = \rho dY_i/dt$ represents the rate of production/consumption of species, and $\bar{R}$ is the specific gas constant. The Lewis number is assumed to be unity which results in $\kappa/c_p = \rho D_i$, hence, the dynamic thermal diffusivity of species is used to model its mass diffusivity.

The equations above are integrated in two dimensions using the Open source Field Operation And Manipulation (OpenFOAM) toolbox [12]. The spatial discretization of the solution domain is done using finite volumes, and the pressure-velocity coupling is achieved using the PIMPLE (PISO+SIMPLE) algorithm. The geometry simulated corresponds to that used in [4], a combustion vessel of 11.4cm x 17.1cm with a glowplug of 9.3mm x 5.1mm located in the center. There are approximately 200k cells in the computational domain, compressed near the wall of the glow plug, with a minimum cell size of 80 μm to allow for enough resolution to resolve the thermal and hydrodynamic boundary layer. Initial conditions are $p_o = 101\,\text{kPa}$, $T_o = 300\,\text{K}$, $U_o = 0\,\text{m/s}$, premixed stoichiometric hydrogen-air mixture ($Y_{H_2} = 0.0283$, $Y_{O_2} = 0.2264$, $Y_{N_2} = 0.7453$), with non-slip and adiabatic boundary condition on walls, and a prescribed temperature ramp (spatially uniform) on the surface of the glowplug given by $T(t) = T_o + rt$ with $r = 220\,\text{K/s}$ as in [4].

3. RESULTS AND DISCUSSION

3.1. Overview, flow structure and temporal evolution

In the present work, numerical simulation of ignition of stoichiometric hydrogen-air mixtures by a rapidly heated commerical glow plug previously studied in experiments by Boettcher [4] is performed.

In particular, one of the observations made by Boettcher suggested an interesting line of further study. According to his experiments with hydrocarbons (n-Hexane), in 53 % of them ignition was observed to occur at the top of the glowplug, 30 % were reported to have taken place on the side of the hot surface, and 17 % in the thermal plume that develops as a consequence of the buoyancy driven flow. Why is ignition more likely to occur at the top? This study aims to answer this question and to understand the physics driving this behavior.

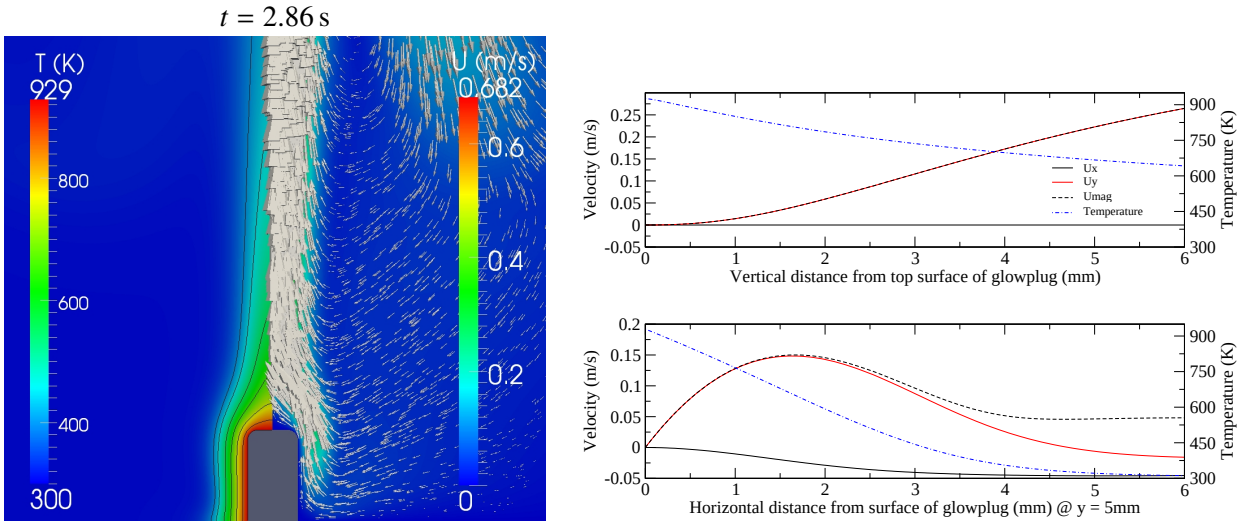

Figure 1: Left: temperature and velocity (magnitude) field in the vicinity of the glowplug, temperature isocontours and velocity vectors. Right: spatial distribution of velocity and temperature at top y = 9.3mm and side y = 5mm of glowplug.

Figure 1 (Left) shows the temperature and velocity (magnitude) fields obtained after 2.86 s of heating, together with temperature isocontours taken every 50 K from 400 K $\leq T \leq$ 930 K, and velocity vectors showing clearly the buoyancy driven flow induced by the glowplug. Figure 1 (Right) shows plots of the spatial distribution of each velocity component, magnitude and temperature at two locations on the glowplug. At the top (y = 9.3 mm) the vertical spatial distribution, and at the side (y = 5 mm) the horizontal spatial distribution. In the vicinity of the hot surface there is development of a thermal boundary layer and thermal plume. Note that in the separated region (top of the glowplug) there is preferential heat diffusion taking place. The thermal plume is delineated by the outermost temperature contour (T = 400 K). The velocity (magnitude) field and velocity vectors show the flow structure near the glowplug. Parcels of fresh cold gas enter the thermal boundary layer from below and heat up slowly as they travel upward in close proximity to the wall. Once they reach the upper right/left corner of the glowplug, the flow separates creating a region at the top of the glow plug where the gas is practically at rest. The gas continues to rise to the top of the combustion vessel, is forced to turn and creates a rather complex vortical flow field, a glimpse of which can be seen on the upper region of the velocity fields. Details of this flow field and an unusual cyclic flame oscillation were examined in experiments and simulations by Boettcher et al. [13] for hexane-air mixtures in this geometry.

In Fig. 1 (right), the horizontal (U_x) and vertical (U_y) components of the velocity vector, black and red solid lines respectively, magnitude (dashed line) and temperature (blue dashed-dotted line) confirm that at up to 0.5 mm away from the top surface of the glowplug the flow is essentially stagnant. As a result, the gas can be readily heated up by the hot surface because convective losses are minimal in this region. This plot also shows the temperature distribution of the thermal plume up to 6 mm away from the glowplug surface. At the side of the glowplug (y = 5 mm), bottom plot on Fig. 1 (Right), the temperature and velocity magnitude plots show the thermal and hydrodynamic boundary layer thickness, 5.5 mm and 4 mm respectively. The negative values of U_x (gas moving left) display how parcels of fluid

are brought into the thermal boundary layer from colder regions away from the glowplug, slowed as they approach the hot surface, changing direction gradually (see increase in U_y), subsequently reaching a maximum, immediately followed by a decrease to zero velocity at the wall consistent with the non-slip condition imposed.

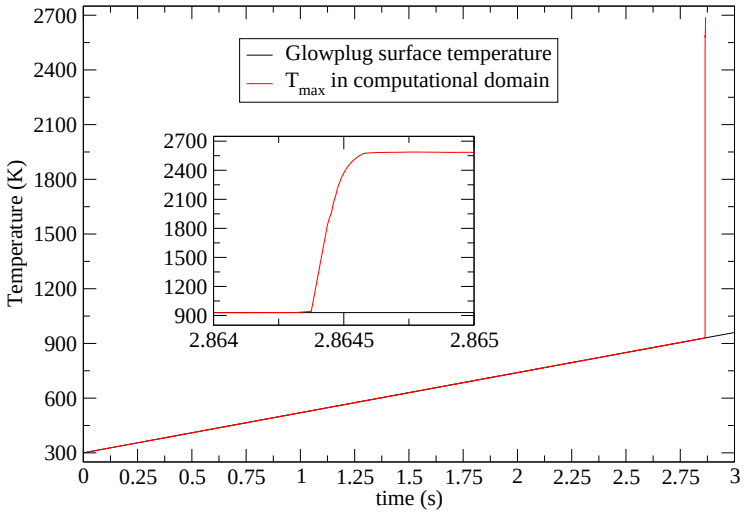

Figure 2: Temperature maximum in computational domain during the course of the simulation. Inset: closeup to ignition event.

To accurately determine the ignition time, τ_{ign}, the temperature maximum in the computational domain and glowplug surface temperature are monitored during the simulation. The inset in Fig. 2 shows a close up of the main heat release event. The time to ignition is $\tau_{ign} = 2.864435$ s. The temperature of the glowplug surface is ~ 930 K at this time. The strong dependence of ignition threshold on temperature is consistent with constant volume explosion simulations for stoichiometric hydrogen-air mixtures. These simulations show a rapid increase in ignition delay times below 1000 K, indicative of a sharp change in activation energy in this temperature range. For instance, the constant volume ignition delay time at 900 K is 94 ms decreasing to 2.09 ms at 930 K.

3.2. Ignition evolution

Figure 3 shows velocity, temperature and product (H_2O) mass fraction fields together with velocity vectors at four instances during the simulation. At $t = 2.86432$ s chemical activity is already taking place at the top of the glowplug where the temperature is highest, and convective losses are minimal. The temperature maximum in the domain ($T = 930$ K) corresponds to that of the glowplug surface until ignition takes place. At $t = 2.864435$ s, 115 μs later, an ignition center appears on the temperature field as closed contours at the top surface of the glowplug. The temperature contours are rescaled to cover the full range of temperature within the computational domain at each time shown in Fig. 3. This ignition center is accompanied by an associated localized increase in H_2O concentration and gas velocity. The velocity vectors show how the ignition kernel abruptly pushes away the surrounding gas. Further acceleration of the gas from 2 m/s to 10 m/s in 28 μs can be seen on the velocity fields at $t = 2.864463$ s. The rapid expansion is evidenced by the size of the velocity vectors. A nascent flame is observed in the temperature contours, and the fuel is nearly completely consumed within the flame kernel, as the mass fraction of H_2O is 0.21 close to the theoretical value of 0.25 given by complete oxidation of a stoichiometric mixture. The last frame shows the early stages of flame propagation, the gas continues to be pushed radially outwards very rapidly, and the shape of the flame is determined by the preferential propagation of the combustion front along the thermal plume where the fresh combustible mixture is

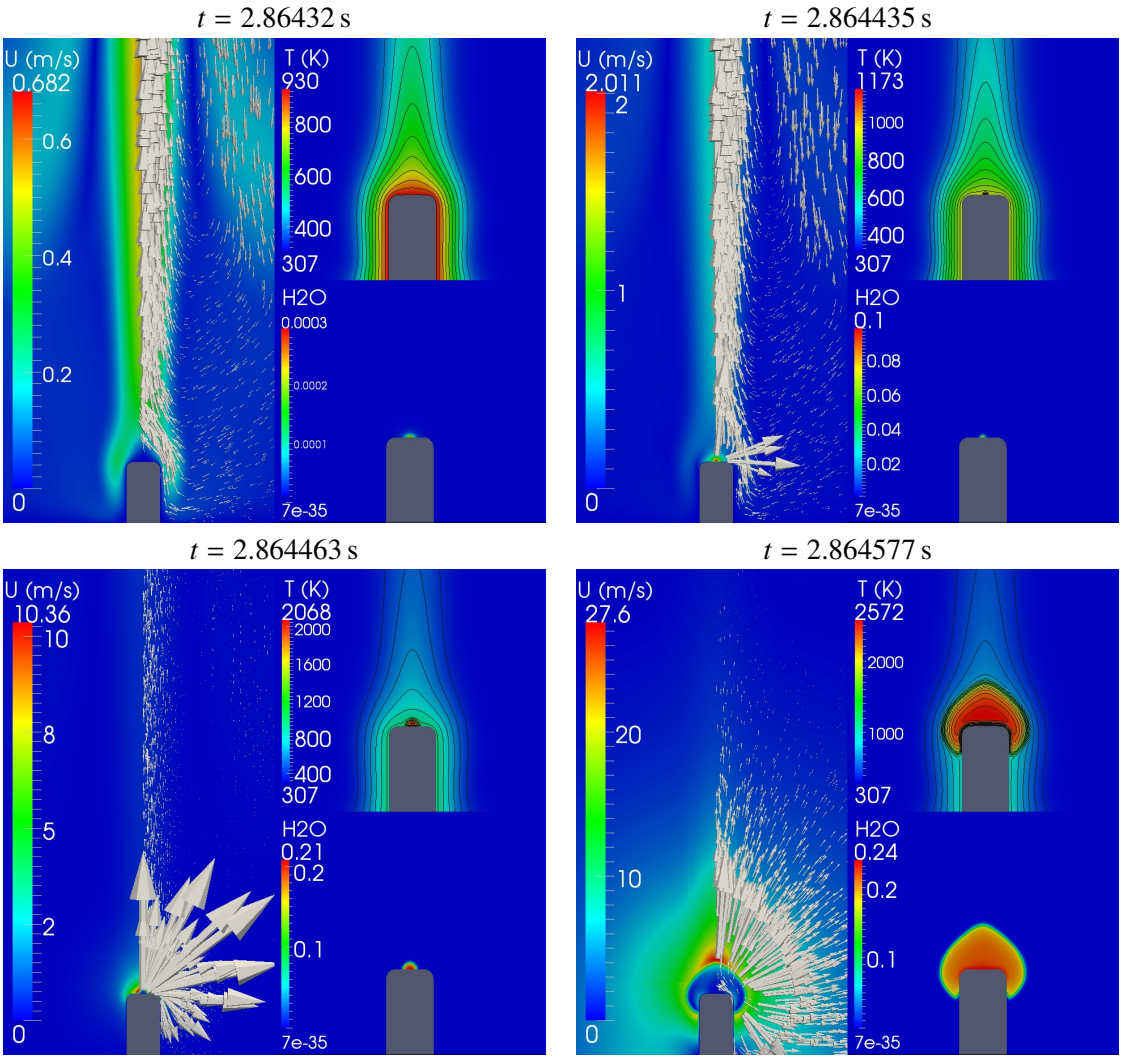

Figure 3: Velocity, product mass fraction and temperature fields. Top Left: at t = 2.86432 s - shortly before ignition. Top Right: at t = 2.864435 s - ignition event. Bottom Left: at t = 2.864463 s - shortly after ignition/flame kernel formation. Bottom right: at t = 2.864577 s - early stages of flame propagation.

hottest. Similar behavior was observed and simulated by Boettcher et al. [13] for the ignition of hexane-air mixtures. The temperature contours show clearly, a nearly uniform high temperature region within the flame.

3.3. Energy equation analysis

To gain additional insight into the processes taking place at the top of the glowplug, each of the terms in the energy conservation equation is plotted along the vertical centerline from the surface of the glowplug (see Figure 4). The plots are taken at the same times as in Figure 3 to allow for a direct comparison. The abscissas represent the normal vertical distance from the surface of the glowplug, whereas the ordinates show the corresponding energy density and temperature. The solid lines are the convective and diffusive heat losses, and the chemical source term given respectively by $h_{Convection} = -\nabla \cdot (\rho \mathbf{u} h)$, $h_{Diffusion} = \nabla \cdot (\kappa / c_p \nabla h)$, and $h_{Source} = q_{chem}$. The dashed line is the sum of the above terms, and the dashed-dotted line is the temperature. Shortly before ignition (Fig. 4 top left), close to the glowplug surface, the source term is mostly balanced by diffusion. The dip in the convective term is due to the expansion of the gas taking place in this area as a result of the initial heat release produced by the chemistry; the sum is positive up to 0.5 mm from the glowplug surface, and the temperature maximum

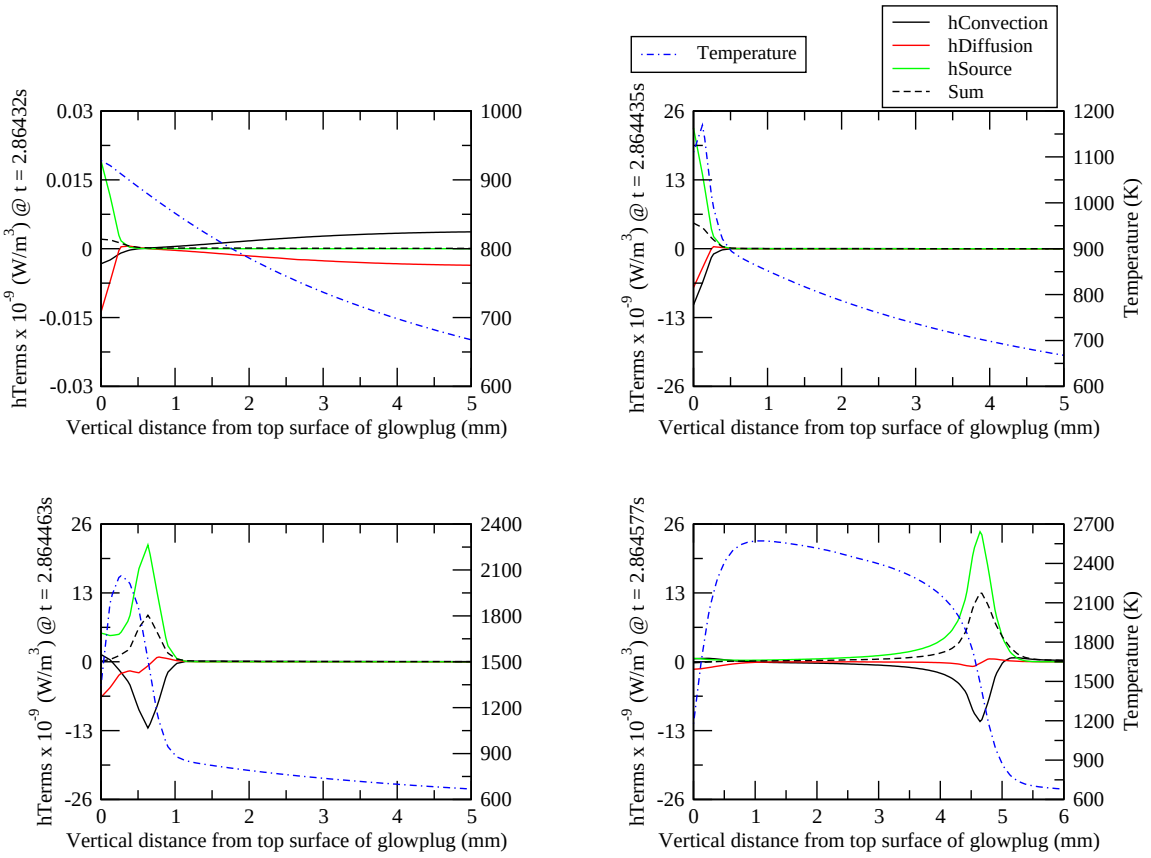

Figure 4: Ignition evolution: contributions of each term in energy equation and temperature along normal distance from top surface of the glowplug. Top Left: at t = 2.86432 s - shortly before ignition. Top Right: at t = 2.864435 s - ignition event. Bottom Left: at t = 2.864463 s - shortly after ignition/flame kernel formation. Bottom right: at t = 2.864577 s - early stages of flame propagation.

remains at the wall. Further away from the glowplug's wall however (0.5 – 5 mm), convection balances diffusion.

In Fig. 4 top right, 115 μs later, the temperature maximum is no longer at the wall but roughly 0.12 mm away from the surface of the glowplug, hence, the rate at which heat is diffused back to the wall is not large enough to counteract the rate at which heat is released by the chemistry at this location, signaling the birth of an ignition center. The explosive nature of the ignition event can be visualized in the increase of over 1000 times in the source term over 115 μs. The bottom left plot of Fig. 4 shows the structure of the ignition center and the birth of an expanding flame kernel. Due to the abrupt expansion of the gas, and associated velocity (10 m/s), the chemical source term is balanced at the flame front ($\sim$ 0.5 mm) mostly by the convective term. At the wall, the balance is maintained by diffusion as expected. The plot at the bottom right of Fig. 4, displays very clearly the structure of the flame propagating away from the surface of the glowplug.

3.4. Chemical pathways

Plotting the contributions of each term in the energy equation and temperature perpendicularly from the top surface of the glowplug was necessary to find the exact location where ignition takes place, $y = 0.12$ mm on the centerline above the glowplug. To investigate the chemistry in more detail, temporal probes were collected for temperature, chemical source term, diffusive and convective losses, together with species profiles. The plots in Figure 5, show the start of heat release as early as $t = 2.86435$ s, diffusion

and convection immediately counteract the source term. The ignition event is marked by the sudden increase in the rate at which energy is deposited in the gas, rise in temperature, rapid consumption of fuel and the production of H_2O and reactive transient species, H, OH and O. Before ignition takes place, at $t = 2.863$ s the species H_2O_2 and HO_2 start to build up. At $t = 2.864$ s, HO_2 increases substantially just before ignition occurs.

Figure 6 displays the reaction pathway diagram. It is seen that the chain branching reactions, R_1: H + O_2 = OH + O and R_2: O + H_2 = OH + H, account only for 15 to 20 % of the reactants consumption. Molecular hydrogen and oxygen are consumed by R_3: H_2 + OH = H_2O + H and R_4: H + O_2(+M) = HO_2(+M), respectively. While R_3 is highly exothermic and induces significant release of energy, R_4 delays the formation of OH radical. Only 34 % of OH is formed by R_1 and R_2, whereas the sequence R_4 followed by R_5: HO_2 + H = OH + OH represents 66 % of OH formation. Under this low temperature conditions, indirect formation of OH radicals through linear chain chemical processes dominates over direct, chain branching reactions. This is consistent with the expected and previously observed behavior of low-temperature homogeneous reaction kinetics.

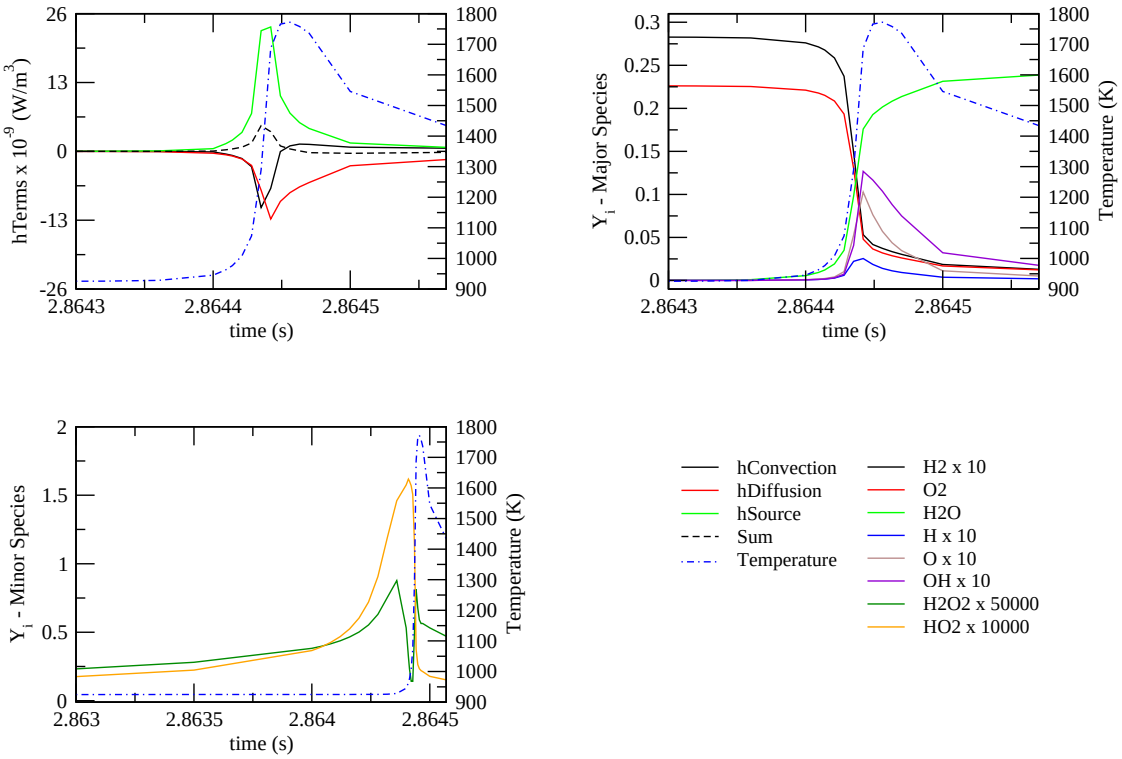

Figure 5: Temporal evolution of each term in energy equation, temperature and species mass fractions at the ignition location, $y = 0.12$ mm.

4. CONCLUSION

Two-dimensional simulations of ignition by a transiently heated commercial glowplug were performed. In agreement with experiments with hydrocarbon-air mixtures, ignition was observed to occur at the top of the glowplug. The details of the ignition kernel evolution was explained by means of velocity, product mass fraction and temperature fields. Additional insight was achieved by analyzing the individual contributions of the terms in the energy conservation equation. Close to the wall, diffusion counteracts

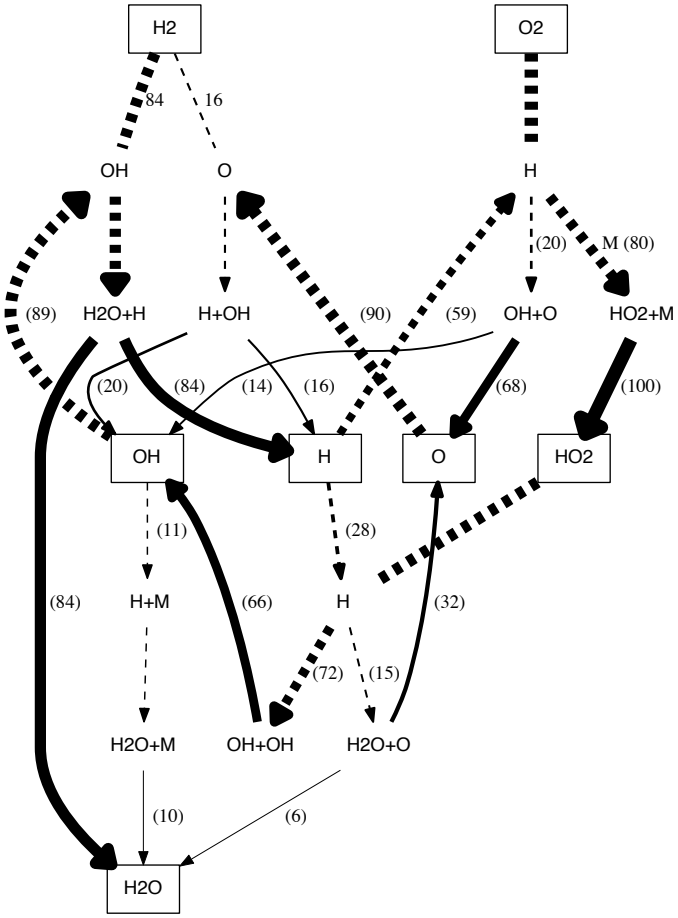

Figure 6: Reaction pathway analysis at the ignition location, $y = 0.12$ mm. Boxes represent species reservoirs, solid lines are reservoir inputs, and dashed lines are reservoirs outputs.

the heat release due to the chemistry, whereas far away, convection and diffusion maintain the balance. Ignition occurs when the heat release rate is greater than the rate at which heat is diffused back to the wall. Results show the importance of flow separation in creating zones that are prone to ignition. Under these thermodynamic conditions, the reaction pathway analysis showed that ignition is essentially driven by a linear chain chemical process. The chain branching reactions, $H + O_2 = OH + O$ and $O + H_2 = OH + H$ constitute minor pathways in producing reactive radicals. The main sequence leading to hydroxyl radical formation is: $H + O_2(+M) = HO_2 + M$; $HO_2 + H = OH + OH$. We anticipate that analogous and much more complex processes also dominate the thermal ignition chemistry of hydrocarbons in this configuration.

ACKNOWLEDGMENTS

This work was carried out in the Explosion Dynamics Laboratory of the California Institute of Technology, J. Melguizo-Gavilanes was supported by the Natural Sciences and Engineering Research Council of Canada (NSERC) Postdoctoral Fellowship Program, and R. Mével by The Boeing Company through a Strategic Research and Development Relationship Agreement CT-BA-GTA-1.

REFERENCES

1. Coward, H.F. and Guest, P.G., Ignition of natural gas-air mixtures by heated metal bars 1, *Journal of the American Chemistry Society*, **1927**, 49(10), pp. 2479-2486
2. Kuchta, J.M., Investigation of fire and explosion accidents in the chemical, mining, and fuel related industries, **1985**, *Bulletin 680, Bureau of Mines*.
3. Brabrauskas, V., Ignition Handbook, **2003**, Fire Science Publishers.
4. Boettcher, P.A., Thermal Ignition, **2012**, Ph.D Thesis. Caltech.
5. Gray, B.F., The dependence of spontaneous ignition temperature on surface to volume ratio in static systems for fuels showing negative temperature coefficient, *Combustion and Flame*, **1970**, 14(1), pp. 113-115
6. Laurendeau, N.M., Thermal ignition of methane-air mixtures by hot surfaces: A critical examination, *Combustion and Flame*, **1982**, 46, pp. 29-49
7. Kumar, R.K., (1989). Ignition of hydrogen-oxygen-diluent mixtures adjacent to a hot, nonreactive surface, *Combustion and Flame*, **1989**, 75(2), pp. 197-215
8. Adler, J., Ignition of a combustible stagnant gas layer by a circular hot spot. *Combustion Theory and Modeling*, **1999**, 3(2), pp. 359-369
9. Boettcher, P.A., Mével, R., Thomas, V. and Shepherd, J.E., (2012). The effect of heating rates on low temperature hexane combustion, *Fuel*, **2012**, 96, pp. 392-403
10. Mével, R., Javoy, S., Lafosse, F., Chaumeix, N., Dupré, G. and Paillard, C.E., Hydrogen-nitrous oxide delay time: shock tube experimental study and kinetic modelling, *Proceedings of The Combustion Institute*, **2009**, 32, pp. 359-366.
11. Mével, R., Javoy, S. and Dupré, G., A chemical kinetic study of the oxidation of silane by nitrous oxide, nitric oxide and oxygen, *Proceedings of The Combustion Institute*, **2011**, 33, pp. 485-492.
12. Weller, H.G., Tabor, G., Jasak, H., and Fureby, C., A tensorial approach to continuum mechanics using object-oriented techniques, *Journal of Computational Physics*, **1998**, 12, pp. 620-631
13. Boettcher, Menon, S.K., Ventura, B.L., Blanquart, G. and Shepherd, J.E., Cyclic Flame Propagation in Premixed Combustion, *Journal of Fluid Mechanics*, **2013**, 735, pp. 176-202